Zinc promotes liquid–liquid phase separation of tau protein

Received for publication, February 21, 2020, and in revised form, March 21, 2020 Published, Papers in Press, March 30, 2020, DOI 10.1074/jbc.AC120.013166

Virender Singh, Ling Xu, Solomiia Boyko, Krystyna Surewicz, and Witold K. Surewicz[1]

From the Department of Physiology and Biophysics, Case Western Reserve University, Cleveland, Ohio 44106

Edited by Ursula Jakob

Tau is a microtubule-associated protein that plays a major role in Alzheimer's disease (AD) and other tauopathies. Recent reports indicate that, in the presence of crowding agents, tau can undergo liquid–liquid phase separation (LLPS), forming highly dynamic liquid droplets. Here, using recombinantly expressed proteins, turbidimetry, fluorescence microscopy imaging, and fluorescence recovery after photobleaching (FRAP) assays, we show that the divalent transition metal zinc strongly promotes this process, shifting the equilibrium phase boundary to lower protein or crowding agent concentrations. We observed no tau LLPS-promoting effect for any other divalent transition metal ions tested, including Mn^{2+}, Fe^{2+}, Co^{2+}, Ni^{2+}, and Cu^{2+}. We also demonstrate that multiple zinc-binding sites on tau are involved in the LLPS-promoting effect and provide insights into the mechanism of this process. Zinc concentration is highly elevated in AD brains, and this metal ion is believed to be an important player in the pathogenesis of this disease. Thus, the present findings bring a new dimension to understanding the relationship between zinc homeostasis and the pathogenic process in AD and related neurodegenerative disorders.

Tau is an intrinsically disordered protein that is involved in microtubule assembly through its positively charged pseudo-repeat domain (1–4). Normally, the protein is in equilibrium between the free and microtubule-bound states. However, under pathological conditions, it aggregates into neurofibrillary tangles, which are one of the hallmarks of Alzheimer's disease (AD)[2] and related tauopathies (1–4). AD is a multifactorial disorder driven by the convergence of many cellular defects that, among other effects, increases aggregation susceptibility of Aβ and tau (5–7). There is growing evidence that zinc level is highly elevated in vulnerable regions of AD brains and that abnormal homeostasis of this metal ion plays an important role in the etiology of the disease (8–12).

Recent reports indicate that, under certain conditions, full-length tau can undergo liquid–liquid phase separation (LLPS), whereby the protein condenses into liquid droplets (13–15). This can occur upon the addition of RNA (13) or, for protein alone, in the presence of crowding agents that mimic high concentration of macromolecules in the intracellular environment (14–16). Even though it was originally suggested that only phosphorylated tau can undergo LLPS in the absence of polyanions such as RNA (14), more recent studies revealed that this process does not require phosphorylation (or any other posttranslational modifications) and that tau LLPS is driven by attractive electrostatic intermolecular interactions between oppositely charged domains of the protein (15). Furthermore, limited observations indicate that tau LLPS may also occur in neurons (14). Because the environment inside phase-separated droplets is distinct from that of the surrounding aqueous phase, LLPS may have a major effect on the formation of pathological protein aggregates in AD and other neurodegenerative disorders (17–20).

Here, we demonstrate that zinc ions can strongly promote LLPS of tau and provide insight into the mechanism of this process. These findings are of potential importance for understanding the pathogenic process in AD.

Results and discussion

Consistent with previously published data (15), in the absence of any crowding agents, freshly prepared solution of tau441 (10 μM) at neutral pH in 10 mM HEPES buffer (pH 7.4) containing 10–150 mM NaCl shows no measurable turbidity, indicating that the protein exists in a single phase, most likely as a monomer (21). However, upon the addition of Zn^{2+} (40 μM) to the protein solution at low ionic strength (10 mM HEPES, 10 mM NaCl, pH 7.4), a large increase in turbidity was observed (Fig. 1*A*), suggesting LLPS. To verify that this effect was indeed due to LLPS (and not protein aggregation), formation of spherical droplets expected for LLPS was directly confirmed by fluorescence microscopy using a mixture of unlabeled tau441 and tau441 labeled with Alexa Fluor 488 (10:1 molar ratio) (Fig. 1*B*). It should be noted that an increase in turbidity of tau solution (in 50 mM Tris buffer) upon zinc addition was also observed in a recent study by Roman *et al.* (22). However, this effect was attributed to oligomerization of the protein, not to LLPS. Thus, to further explore the nature of spherical droplets observed in our study, we used time-lapse microscopy to demonstrate that these droplets undergo fusion (Fig. 2*A*). Furthermore, fluorescence recovery after photobleaching (FRAP) experiments revealed rapid recovery of the fluorescence signal, indicating fast protein diffusion that was maintained for at least 2 h after droplet formation (Fig. 2*B*). Altogether, these experiments clearly demonstrate that tau441 in the presence of zinc ions

This work was supported by National Institutes of Health Grant RF1 AG061797 (to W. K. S.) and the Department of Physiology and Biophysics, Case Western Reserve University, Pilot Project Grant (to W. K. S.). The authors declare that they have no conflicts of interest with the contents of this article. The content is solely the responsibility of the authors and does not necessarily represent the official views of the National Institutes of Health.
This article was selected as one of our Editors' Picks.
This article contains Figs. S1–S4.

[1] To whom correspondence should be addressed. Tel.: 216-368-0139; E-mail: witold.surewicz@case.edu.

[2] The abbreviations used are: AD, Alzheimer's disease; LLPS, liquid–liquid phase separation; FRAP, fluorescence recovery after photobleaching; OD, optical density.

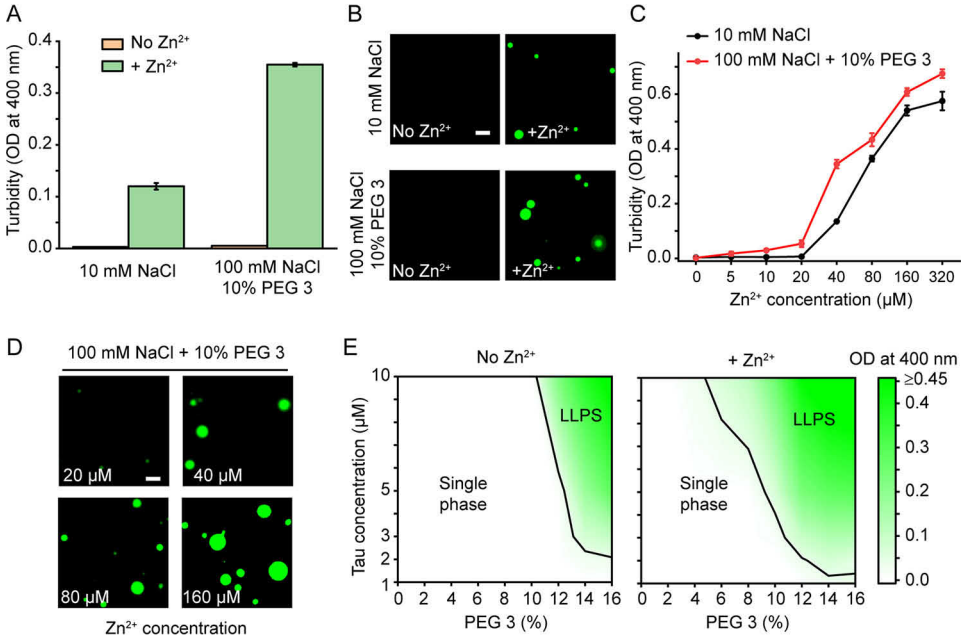

Figure 1. Zinc promotes LLPS of tau441. *A*, LLPS of tau441 (10 μM) in the absence (*orange*) or presence of $ZnCl_2$ (40 μM; *green*) monitored by turbidity (OD at 400 nm). Experiments at low ionic strength (10 mM NaCl) were performed without any crowding agent, and experiments at higher ionic strength (100 mM NaCl) were performed in the presence of 10% PEG 3. *Error bars*, S.D. ($n = 5$). *B*, representative fluorescence microscopy images of tau441 (10 μM) in the absence and presence of Zn^{2+} (40 μM) in the same buffers as described in *A*. The images were obtained using Alexa Fluor 488–labeled tau441 that was added to the solution of unlabeled protein at a molar ratio of 1:10. *Scale bar*, 5 μm. *C*, turbidity of tau441 (10 μM as a function of Zn^{2+} concentration in a buffer containing 10 mM NaCl (*black*) and 100 mM NaCl + 10% PEG 3 (*red*). *Error bars*, S.D. ($n = 5$). *D*, representative fluorescence microscopy images of tau441 (10 μM) as a function of Zn^{2+} concentration in a buffer containing 100 mM NaCl and 10% PEG 3. *Scale bar*, 5 μm. *E*, phase diagrams of tau441 in a buffer containing 100 mM NaCl and in the absence and presence of zinc (Zn^{2+}/protein molar ratio of 4:1). *Color coding* represents average turbidity (OD at 400 nm) ($n = 5$). *Black lines* indicate the liquid–liquid phase boundaries defined as OD of 0.04 (which corresponds to the threshold of OD increase that could be reproducibly determined in these experiments).

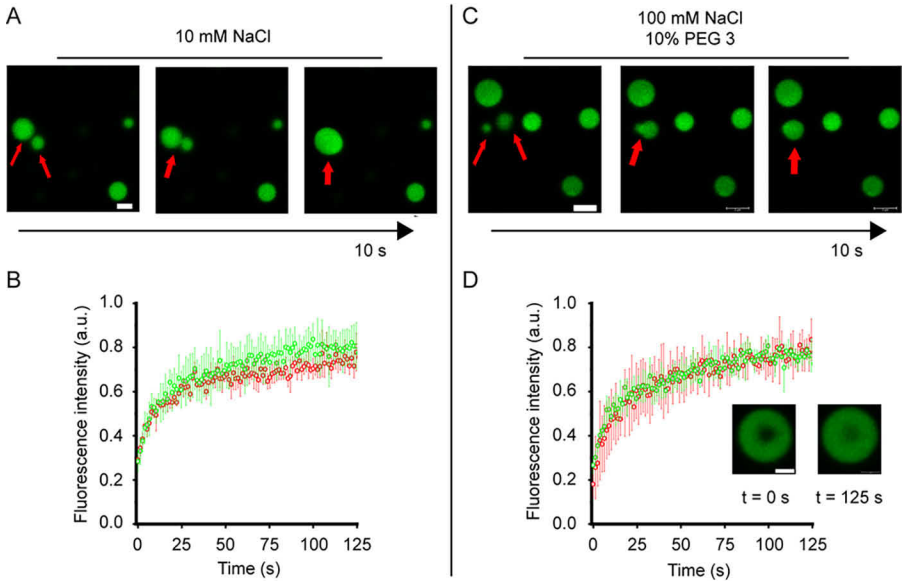

Figure 2. Zinc-induced tau441 droplets are liquid-like. *A*, representative fusion events between tau441 (10 μM) droplets induced by 40 μM zinc (Zn^{2+}/tau441 molar ratio of 4:1) in low-ionic strength buffer (10 mM HEPES, 10 mM NaCl, pH 7.4) without any crowding agent. *Scale bar*, 2 μm. *B*, FRAP traces for tau441 droplets in low-ionic strength buffer (10 mM NaCl, no crowding agent) obtained 10 min (*red*) and 120 min (*green*) after inducing LLPS with 40 μM Zn^{2+}. *C*, representative fusion events between tau441 (10 μM) droplets induced by 40 μM zinc (Zn^{2+}/tau441 molar ratio of 4:1) in a buffer containing 100 mM NaCl and 10% PEG 3. *Scale bar*, 2 μm. *D*, FRAP traces for tau droplets in a buffer containing 100 mM NaCl and 10% PEG 3 obtained 10 min (*red*) and 120 min (*green*) after inducing LLPS with 40 μM Zn^{2+}. *Inset*, images of droplets at 0 and 125 s after photobleaching (*scale bar*, 1 μm). *Error bars*, S.D. ($n = 4$).

undergoes LLPS, forming highly dynamic liquid droplets that retain their liquid-like character for several hours after induction.

The capacity of Zn^{2+} to induce LLPS of tau441 diminished with increasing ionic strength of the buffer (Fig. S1, *A* and *B*). However, this capacity could be restored in the presence of crowding agents such as PEG. For example, in the presence of 10% 3-kDa PEG (PEG 3), droplet formation in a Zn^{2+}-containing buffer could be observed at NaCl concentrations at least up to 150 mM (*i.e.* under the conditions where no LLPS was detect-

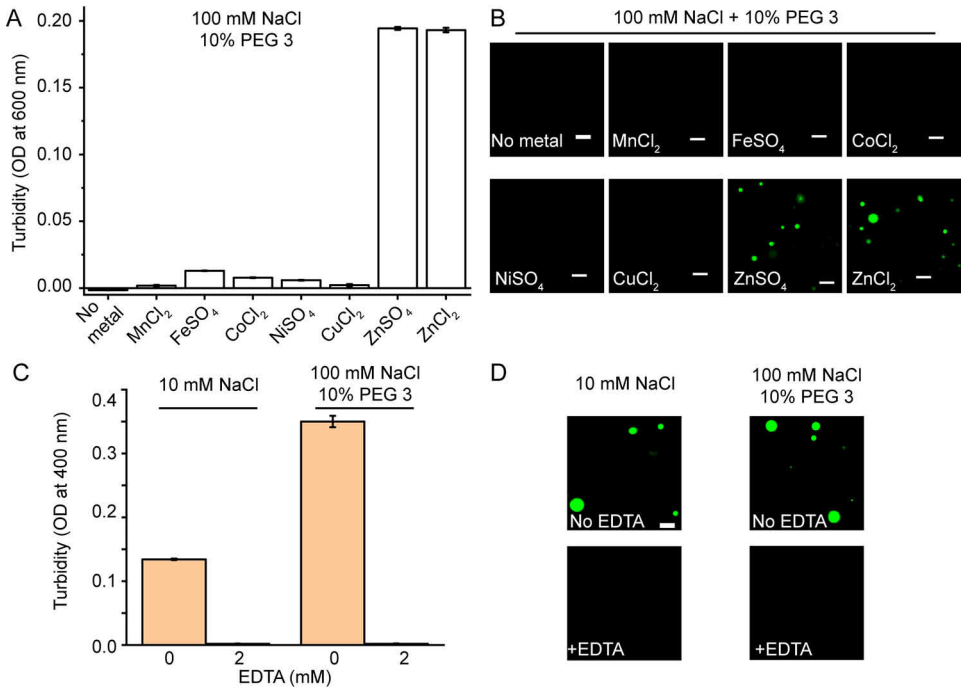

Figure 3. Zinc is specific among divalent transition metal ions in its ability to promote LLPS of tau441. *A*, turbidity (OD at 600 nm) of tau441 (10 μM) in the presence of different transition metal salts (40 μM each) in a buffer containing 100 mM NaCl and 10% PEG 3. *Error bars*, S.D. ($n = 5$). *B*, representative fluorescence microscopy images of tau441 (10 μM) in the presence of different metal salts (40 μM each). The images were obtained at 37 °C in a buffer containing 100 mM NaCl and 10% PEG 3. *Scale bars*, 5 μm. *C*, turbidity (OD at 400 nm) of tau441 (10 μM) in low (10 mM NaCl) and high (100 mM NaCl, 10% PEG 3) ionic strength buffers containing 40 μM Zn^{2+} in the absence (*orange*) and presence (*green*) of 2 mM EDTA. *Error bars*, S.D. ($n = 5$). *D*, representative fluorescence microscopy images of tau441 (10 μM) in low (10 mM NaCl) and high (100 mM NaCl, 10% PEG 3) ionic strength buffers containing 40 μM Zn^{2+} in the absence (*orange*) and presence (*green*) of 2 mM EDTA. *Scale bar*, 5 μm.

able in the absence of zinc ions) (Fig. 1 (*A* and *B*) and Fig. S1 (*C* and *D*)). Again, these droplets were highly dynamic, as indicated by FRAP experiments (Fig. 2*D*) and the ability to undergo fusion (Fig. 2*C*).

Both at low ionic strength (in the absence of any crowding agents) and at higher ionic strength (in the presence of PEG 3), significant LLPS was observed only above the threshold Zn^{2+} to tau441 molar ratio of ~2:1, and the extent of LLPS was gradually increasing with increasing concentration of zinc ions (Fig. 1, *C* and *D*). Data obtained in a buffer containing 100 mM NaCl at various protein and PEG 3 concentrations in the absence and presence of zinc (Zn^{2+}/tau441 molar ratio of 4:1) are summarized in the form of phase diagrams shown in Fig. 1*E*. These phase diagrams clearly demonstrate that zinc ions strongly enhance the propensity for tau to form a two-phase system, shifting the equilibrium phase boundary to lower protein or crowding agent concentrations. For example, in a buffer containing 100 mM NaCl and 12% PEG 3 (*i.e.* within the range of PEG concentrations typically used to mimic intracellular molecular crowding (23)), significant LLPS in the presence of zinc was observed at tau441 concentration as low as 2 μM. In contrast, LLPS in the absence of zinc could be detected only at tau441 concentrations above ~5 μM (Fig. 1*E*). To put this in a physiological context, intracellular tau concentrations are estimated to be between ~2 and 7 μM (14). A similar LLPS-promoting effect of Zn^{2+} was observed when higher-molecular weight PEG 10, a more potent crowding agent employed in previous studies on tau LLPS (15) was used (Fig. S2).

Next, we asked the question of whether the LLPS-promoting effect of Zn^{2+} described above is representative of all divalent transition metal ions or if it is rather zinc-specific. Surprisingly, none of other divalent transition metal ions tested (Mn^{2+}, Fe^{2+}, Co^{2+}, Ni^{2+}, and Cu^{2+}) was found to facilitate phase separation of tau441 in high or low ionic strength buffer, at least at zinc concentration up to 40 μM (Fig. 3 (*A* and *B*) and Fig. S3). This indicates that these other transition metal ions have much lower (if any) capacity to promote tau LLPS. Furthermore, the effect of Zn^{2+} appears to be independent of the zinc salt's component anion, as $ZnSO_4$ and $ZnCl_2$ have an essentially identical capacity to facilitate LLPS of tau441 (Fig. 3, *A* and *B*). We also verified that, as expected, the addition of a metal-chelating agent, EDTA, completely abrogated Zn^{2+}-induced LLPS of the protein (Fig. 3, *C* and *D*).

Tau441 consists of the negatively charged N-terminal region (that contains two inserts, N1 and N2), a proline-rich region, and four pseudo-repeats flanked by the C-terminal residues (Fig. 4*A*). Both the proline-rich region and the pseudo-repeats are highly enriched in positively charged residues, whereas the most C-terminal part has an overall negative charge. The four pseudo-repeats are known to be essential for microtubule binding as well as pathological aggregation of tau (1, 2). To determine the role of individual tau441 regions in Zn^{2+}-induced LLPS, we employed a number of deletion/substitution variants and fragments of tau441 (Fig. 4*A*).

First, we focused on the pseudo-repeat region (4R), finding that the deletion of this entire domain was sufficient to completely abrogate the ability of zinc to facilitate LLPS, as indicated both by turbidity data (Fig. 4*B*) and fluorescence microscopy (Fig. 4*C*). Given that Cys residues present in the pseudo-repeat region (Cys-291 in R2 and Cys-322 in R3) were

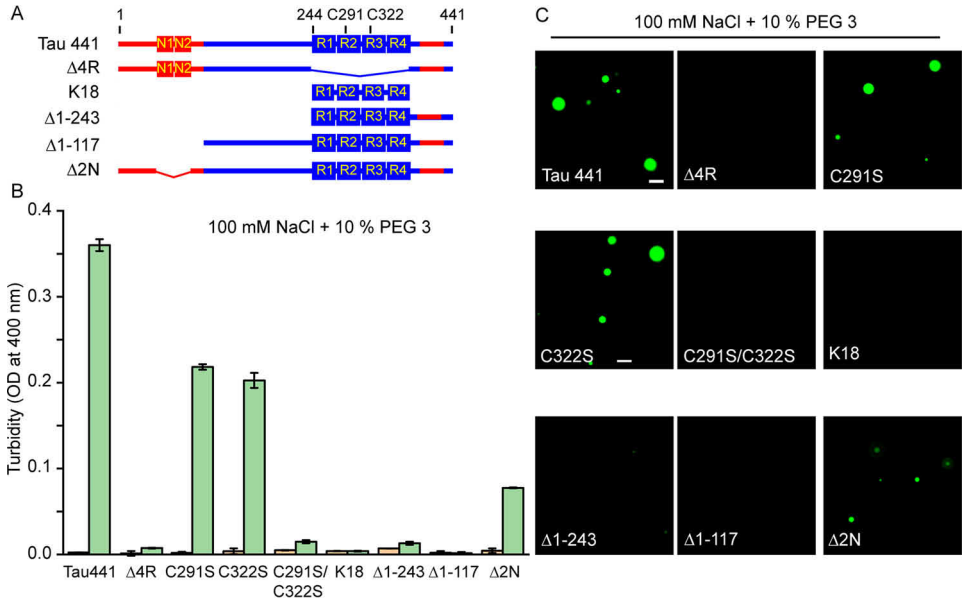

Figure 4. The role of individual regions of tau and Cys residues in zinc-induced LLPS. *A*, *schematic diagram* of tau deletion/truncation variants used in this study. The basic and acidic regions are *marked* in *blue* and *red*, respectively. *B*, turbidity (OD at 400 nm) of different tau variants (10 μM each in a buffer containing 100 mM NaCl and 10% PEG 3) in the absence (*orange*) and presence (*green*) of 40 μM Zn^{2+}. *Error bars*, S.D. ($n = 5$). *C*, representative fluorescence microscopy images of different tau variants (10 μM each) in the presence of 40 μM Zn^{2+}. The images were recorded in a buffer containing 100 mM NaCl and 10% PEG 3. *Scale bar*, 5 μm.

previously reported to be important for zinc binding to tau (24), next we tested the role of these residues in LLPS. Replacement of either Cys-291 or Cys-322 alone with Ser partially diminished the ability for Zn^{2+} to induce LLPS (although droplets were still visualized by microscopy, a lower turbidity as compared with WT full-length protein was observed). However, substitution of both of these cysteines completely abrogated the ability of zinc ions to induce droplet formation (Fig. 4).

Despite the critical role of Cys residues within the pseudo-repeat region in Zn^{2+}-induced LLPS of full-length tau, neither the isolated pseudo-repeat segment (K18 fragment) nor the longer fragment containing both the pseudo-repeat region and C-terminal residues (Δ1–243tau) was able to undergo LLPS in the presence of zinc ions under the experimental conditions used in the present study. This indicates that additional tau regions are important for this process. To further explore this issue, we performed experiments with the N-terminally truncated variant tauΔ1–117 (in which the entire negatively charged segment has been deleted), finding that Zn^{2+} ions were no longer able to facilitate LLPS of this protein (Fig. 4). Finally, the deletion of only part of the negatively charged region (Δ2N variant in which residues 45–103 are missing) resulted in a partial abrogation of Zn^{2+}-induced LLPS, as indicated by smaller turbidity increase as compared with that observed for full-length tau441 (Fig. 4).

The previous study (15) (performed using similar experimental conditions but a more potent crowding agent, PEG 10) revealed that, in the absence of zinc, the N-terminally truncated tau441 variants Δ1–243 and Δ1–117 as well as the K18 fragment lost the ability to undergo LLPS, whereas the propensity of the Δ2N and Δ4R variants for LLPS was diminished (but not completely abrogated), as indicated by the requirement for higher concentrations of the crowding agent compared with that for tau441. This, together with data shown herein in Fig. 4*B*, suggests that zinc can promote LLPS only for those tau variants that have an intrinsic propensity to undergo phase separation even in the absence of the metal ion. To further probe this issue and conclusively establish the role of Cys residues in the LLPS-promoting effect of zinc, we performed additional experiments in the presence of 12% PEG 3 (*i.e.* under conditions that lead to partial LLPS of the full-length protein and some of its variants in the absence of zinc). As shown in Fig. S4, also under these conditions, zinc partially retained the ability to further promote LLPS of the Δ2N and single-Cys variants, but completely lost the ability to facilitate LLPS of the Δ4R and C291S/C322S variants. Thus, the presence of at least one Cys residue is crucial for this effect. This is in line with the finding that substitution of individual Cys residues in a tau fragment encompassing residues 244–372 only modestly decreases the affinity for Zn^{2+}, whereas substitution of both of them totally abrogates this binding (24).

Altogether, the present data clearly demonstrate that zinc strongly promotes LLPS of full-length tau and identify specific structural elements within the protein that are important for this effect. The finding that Cys residues are essential for Zn^{2+}-induced LLPS is consistent with previous isothermal titration calorimetry studies that identified a single high-affinity binding site (with reported K_d between 0.5 and 4 μM) in which zinc is coordinated by two Cys and two His residues (His-330 and His-362) within the R2-R3 tau region (22, 24). However, this high-affinity binding appears to be insufficient to promote LLPS, as zinc-induced droplet formation was observed only at Zn^{2+}/tau441 molar ratios above 2:1. This conundrum may be explained by the most recent finding that, in addition to the high binding site, tau contains three low-affinity zinc-binding sites, with an average K_d around 20 μM (22). These low-affinity binding sites appear to be also essential for zinc's ability to promote LLPS of tau. Even though the nature of the latter binding

sites is at present unknown, they likely involve His residues outside the pseudo-repeat region as well as Asp and Glu residues (25). The latter residues, known to be involved in binding of transition metal ions (25–27), are especially abundant in the negatively charged N-terminal region of tau. The finding that the extent of tau LLPS gradually increases at zinc concentrations corresponding to Zn^{2+}/tau molar ratios above 4:1 (Fig. 1*D*) suggests that at least some of the low-affinity binding sites become populated only at zinc concentration higher than expected for the reported average K_d value of ~20 μM (22).

Even though the LLPS-promoting effect of zinc is critically dependent on the presence of at least one Cys residue within the pseudo-repeat region, the latter region alone appears to be insufficient to support this effect, as the K18 fragment was not able to undergo LLPS, even at high zinc concentrations. It should be noted that droplet formation by K18 (in the absence of zinc) was previously reported (28, 29). However, this was observed only upon many hours of incubation at high protein concentration (~100 μM) in a pH 8.8 buffer (*i.e.* near the isolelectric point of the K18 fragment). No LLPS of K18 (in the absence or presence of zinc) was observed under physiologically more relevant conditions used in the present study.

Our previously published data revealed that LLPS of tau without zinc—which under similar crowding conditions requires substantially higher protein concentrations than in the presence of Zn^{2+}—is largely driven by attractive intermolecular electrostatic interactions between the negatively charged N-terminal and positively charged middle/C-terminal regions of the protein (15). The salt dependence and experiments employing tau variants with partial (Δ2N, Δ1–117) or complete (Δ1–243) deletions of the negatively charged N-terminal region indicate that similar electrostatic interactions are also operational in Zn^{2+}-mediated LLPS. Thus, what is the mechanism by which zinc promotes this process? Certain clues in this regard are provided by the finding that zinc binding results in a more compact structure of tau monomers (22), suggesting that coordination through Cys and His residues induces local hairpin-like folding within the pseudo-repeat region (22, 25). A similar local folding has also been suggested for the acidic N-terminal region that contains many potential zinc chelating amino acids (25). We propose that this local folding could result in an increased density of positive and negative charges within the pseudo-repeat and N-terminal regions, respectively. This, in turn, would lead to stronger attractive intermolecular interactions, facilitating liquid–liquid phase separation. Another, nonmutually exclusive possibility is that zinc could promote LLPS by facilitating formation of transient intermolecular cross-links between tau molecules. Further studies are needed to explore these (and other) possibilities.

Zinc is the most abundant trace metal ion in brain; it is estimated that activation of zinc-containing presynaptic terminals results in transient local concentration of this metal ion in the 10^{-4} M range (8–10). Furthermore, numerous reports point to an elevated zinc concentration in AD brain, with an especially high level of zinc found around neurofibrillary tangles and Aβ-amyloid plaques (8, 11, 30, 31). Thus, it has been widely postulated that zinc may play an important role in AD and other neurodegenerative diseases (9, 12, 31). One possible mechanism by which zinc could exert this effect is by increasing the aggregation propensity of proteins such as Aβ and tau, and such effects have indeed been observed in experiments *in vitro* (24, 32–35). However, accelerated tau fibrillization was observed only in the presence of nonphysiological cofactors such as heparin (24) or Congo red (33). The present finding that zinc strongly promotes tau LLPS brings a new dimension to understanding the link between abnormal zinc homeostasis and the pathogenic process in AD and other tauopathies, especially because recent data indicate that the environment of liquid droplets strongly modulates the aggregation behavior of several proteins involved in neurodegenerative disorders (14, 18–20, 28, 36, 37). Furthermore, growing data indicate that pathophysiology and toxicity of tau may be mediated by interaction with RNA-binding proteins, such as T-cell intracellular antigen 1 (TIA1) (38, 39). Interestingly, it was recently reported that zinc promotes LLPS of TIA1 under cellular stress conditions (40). Thus, the present evidence that zinc can also induce LLPS of tau suggest that this metal ion may act as a powerful mediator facilitating the interaction of both proteins within the context of stress granules.

Experimental procedures

Expression, purification, and labeling of tau variants

Tau variants used in the present study were expressed and purified as described previously (15). The identity of individual variants was confirmed by electrospray ionization MS. Protein concentration was determined using a reducing agent–compatible Pierce microplate BCA protein assay kit (Thermo Scientific). Proteins were fluorescently labeled with Alexa Fluor 488 dye (Invitrogen) as described previously (15). Labeling efficiency was determined by UV-visible absorption spectroscopy.

Turbidity measurements

LLPS was monitored by turbidity. In most cases, this was done by measuring optical density at 400 nm. The exceptions were the experiments shown in Fig. 3, in which case optical density at 600 nm was used to avoid interference from absorbance by metal ions other than zinc. These measurements were performed at 37 °C using the Tecan Spark plate reader. Experiments at low ionic strength were carried out in 10 mM HEPES buffer (pH 7.4) containing 2 mM tris(2-carboxyethyl)phosphine, 0.02% sodium azide, and 10 mM NaCl. Experiments at higher ionic strength were performed in the same buffer, but containing 100 mM NaCl and 10% PEG with a molecular mass of 3350 (PEG 3; Sigma). Before use, PEG 3 was pretreated with Chelex 100 sodium base (Sigma–Aldrich) to remove residual metal impurities. Phase diagrams shown in Fig. 1*E* were constructed based on turbidity data using a contour-color fill module of the Origin software.

Fluorescence microscopy imaging

Droplets were visualized using a Keyence BZ-X710 inverted fluorescence phase-contrast microscope equipped with a ×100 oil-immersion objective lens (1.45 numerical aperture). For these experiments, unlabeled protein was mixed with Alexa Fluor 488–labeled protein at a 10:1 molar ratio. Samples (20 μl)

were placed on a hydrophobic bottom surface of 35-mm fluorodish, covered with a coverglass, and sealed with nail polish to prevent evaporation. For hydrophobic coating, the dish was covered with 1% Pluronic F-127 (Sigma), incubated for 1 h, and dried under nitrogen. The measurements were performed at 37 °C within 10 min after droplet induction, except for the aging experiment, in which case samples were incubated at 37 °C in 1.5-ml black tubes for 2 h. Images were captured in solution away from the bottom of the dish.

FRAP

FRAP experiments were performed using a Leica HyVolution SP8 confocal microscope equipped with 2.4-milliwatt laser (488 nm), ×63 oil immersion objective (1.4 numerical aperture), and a photomultiplier tube detector. For each experiment, four droplets with 2.5–3.5-μm diameter were selected. A circular region of interest (0.25-μm diameter) was bleached once using 100% laser power. Fluorescence intensity changes with time were recorded for 10 prebleaching frames and 100 post-bleaching frames (1.3 s/frame). Data were analyzed using Leica LAX suite software. At each time point, mean intensities of bleached region (I_R) and neighboring unbleached region (I_U) within the same droplet were measured, and recovered intensity ratios (I_t) were calculated as ($[I_R]/[I_U]$).

Data availability

All data are contained within this article and the supporting information.

Author contributions—V. S. and W. K. S. conceptualization; V. S. data curation; V. S. and W. K. S. formal analysis; V. S. and W. K. S. writing-original draft; V. S., S. B., and W. K. S. writing-review and editing; L. X., S. B., and K. S. resources; W. K. S. supervision; W. K. S. funding acquisition; W. K. S. validation; W. K. S. project administration.

Acknowledgments—We thank Michael Babinchak for critically reading the manuscript. The confocal microscopy facility used in this study was supported by National Institutes of Health Grant S10-OD024996.

References

1. Wang, Y., and Mandelkow, E. (2016) Tau in physiology and pathology. *Nat. Rev. Neurosci.* **17,** 5–21 CrossRef Medline
2. Mandelkow, E. M., and Mandelkow, E. (2012) Biochemistry and cell biology of tau protein in neurofibrillary degeneration. *Cold Spring Harb. Perspect. Med.* **2,** a006247 CrossRef Medline
3. Ballatore, C., Lee, V. M. Y., and Trojanowski, J. Q. (2007) Tau-mediated neurodegeneration in Alzheimer's disease and related disorders. *Nat. Rev. Neurosci.* **8,** 663–672 CrossRef Medline
4. Guo, T., Noble, W., and Hanger, D. P. (2017) Roles of tau protein in health and disease. *Acta Neuropathol.* **133,** 665–704 CrossRef Medline
5. Huang, Y., and Mucke, L. (2012) Alzheimer mechanisms and therapeutic strategies. *Cell* **148,** 1204–1222 CrossRef Medline
6. De Strooper, B. (2010) Proteases and proteolysis in Alzheimer disease: a multifactorial view on the disease process. *Physiol. Rev.* **90,** 465–494 CrossRef Medline
7. Tönnies, E., and Trushina, E. (2017) Oxidative stress, synaptic dysfunction, and Alzheimer's disease. *J. Alzheimers Dis.* **57,** 1105–1121 CrossRef Medline
8. Cuajungco, M. P., and Lees, G. J. (1997) Zinc and Alzheimer's disease: is there a direct link? *Brain Res. Rev.* **23,** 219–236 CrossRef Medline
9. Portbury, S. D., and Adlard, P. A. (2017) Zinc signal in brain diseases. *Int. J. Mol. Sci.* **18,** E2506 CrossRef Medline
10. Szewczyk, B. (2013) Zinc homeostasis and neurodegenerative disorders. *Front. Aging Neurosci.* **5,** 33 CrossRef Medline
11. Frederickson, C. J., Koh, J.-Y., and Bush, A. I. (2005) The neurobiology of zinc in health and disease. *Nat. Rev. Neurosci.* **6,** 449–462 CrossRef Medline
12. Morris, D. R., and Levenson, C. W. (2017) Neurotoxicity of zinc. in *Neurotoxicity of Metals* (Aschner, M., and Costa, L. G., eds) pp. 303–312, Springer International Publishing, Cham, Switzerland
13. Zhang, X., Lin, Y., Eschmann, N. A., Zhou, H., Rauch, J. N., Hernandez, I., Guzman, E., Kosik, K. S., and Han, S. (2017) RNA stores tau reversibly in complex coacervates. *PLoS Biol.* **15,** e2002183 CrossRef Medline
14. Wegmann, S., Eftekharzadeh, B., Tepper, K., Zoltowska, K. M., Bennett, R. E., Dujardin, S., Laskowski, P. R., MacKenzie, D., Kamath, T., Commins, C., Vanderburg, C., Roe, A. D., Fan, Z., Molliex, A. M., Hernandez-Vega, A., Muller, D., *et al.* (2018) Tau protein liquid–liquid phase separation can initiate tau aggregation. *EMBO J.* **37,** e98049 CrossRef Medline
15. Boyko, S., Qi, X., Chen, T.-H., Surewicz, K., and Surewicz, W. K. (2019) Liquid-liquid phase separation of tau protein: the crucial role of electrostatic interactions. *J. Biol. Chem.* **294,** 11054–11059 CrossRef Medline
16. Hernández-Vega, A., Braun, M., Scharrel, L., Jahnel, M., Wegmann, S., Hyman, B. T., Alberti, S., Diez, S., and Hyman, A. A. (2017) Local nucleation of microtubule bundles through tubulin concentration into a condensed tau phase. *Cell Rep.* **20,** 2304–2312 CrossRef Medline
17. Nedelsky, N. B., and Taylor, J. P. (2019) Bridging biophysics and neurology: aberrant phase transitions in neurodegenerative disease. *Nat. Rev. Neurol.* **15,** 272–286 CrossRef Medline
18. Elbaum-Garfinkle, S. (2019) Matter over mind: liquid phase separation and neurodegeneration. *J. Biol. Chem.* **294,** 7160–7168 CrossRef Medline
19. Babinchak, W. M., Haider, R., Dumm, B. K., Sarkar, P., Surewicz, K., Choi, J.-K., and Surewicz, W. K. (2019) The role of liquid-liquid phase separation in aggregation of the TDP-43 low complexity domain. *J. Biol. Chem.* **294,** 6306–6317 CrossRef Medline
20. Molliex, A., Temirov, J., Lee, J., Coughlin, M., Kanagaraj, A. P., Kim, H. J., Mittag, T., and Taylor, J. P. (2015) Phase separation by low complexity domains promotes stress granule assembly and drives pathological fibrillization. *Cell* **163,** 123–133 CrossRef Medline
21. Chirita, C. N., Congdon, E. E., Yin, H., and Kuret, J. (2005) Triggers of full-length tau aggregation: a role for partially folded intermediates. *Biochemistry* **44,** 5862–5872 CrossRef Medline
22. Roman, A. Y., Devred, F., Byrne, D., La Rocca, R., Ninkina, N. N., Peyrot, V., and Tsvetkov, P. O. (2019) Zinc induces temperature-dependent reversible self-assembly of tau. *J. Mol. Biol.* **431,** 687–695 CrossRef Medline
23. Fulton, A. B. (1982) How crowded is the cytoplasm? *Cell* **30,** 345–347 CrossRef Medline
24. Mo, Z.-Y., Zhu, Y.-Z., Zhu, H.-L., Fan, J.-B., Chen, J., and Liang, Y. (2009) Low micromolar zinc accelerates the fibrillization of human tau via bridging of Cys-291 and Cys-322. *J. Biol. Chem.* **284,** 34648–34657 CrossRef Medline
25. Fichou, Y., Al-Hilaly, Y. K., Devred, F., Smet-Nocca, C., Tsvetkov, P. O., Verelst, J., Winderickx, J., Geukens, N., Vanmechelen, E., Perrotin, A., Serpell, L., Hanseeuw, B. J., Medina, M., Buée, L., and Landrieu, I. (2019) The elusive tau molecular structures: can we translate the recent breakthroughs into new targets for intervention? *Acta Neuropathol. Commun.* **7,** 31 CrossRef Medline
26. Breydo, L., and Uversky, V. N. (2011) Role of metal ions in aggregation of intrinsically disordered proteins in neurodegenerative diseases. *Metallomics* **3,** 1163–1180 CrossRef Medline
27. Faller, P., Hureau, C., and La Penna, G. (2014) Metal ions and intrinsically disordered proteins and peptides: from Cu/Zn amyloid-β to general principles. *Acc. Chem. Res.* **47,** 2252–2259 CrossRef Medline
28. Ambadipudi, S., Biernat, J., Riedel, D., Mandelkow, E., and Zweckstetter, M. (2017) Liquid–liquid phase separation of the microtubule-binding repeats of the Alzheimer-related protein Tau. *Nat. Commun.* **8,** 275 CrossRef Medline

29. Ambadipudi, S., Reddy, J. G., Biernat, J., Mandelkow, E., and Zweckstetter, M. (2019) Residue-specific identification of phase separation hot spots of Alzheimer's-related protein tau. *Chem. Sci.* **10,** 6503–6507 CrossRef Medline
30. Suh, S. W., Jensen, K. B., Jensen, M. S., Silva, D. S., Kesslak, P. J., Danscher, G., and Frederickson, C. J. (2000) Histochemically-reactive zinc in amyloid plaques, angiopathy, and degenerating neurons of Alzheimer's diseased brains. *Brain Res.* **852,** 274–278 CrossRef Medline
31. Religa, D., Strozyk, D., Cherny, R. A., Volitakis, I., Haroutunian, V., Winblad, B., Naslund, J., and Bush, A. I. (2006) Elevated cortical zinc in Alzheimer disease. *Neurology* **67,** 69–75 CrossRef Medline
32. Miller, Y., Ma, B., and Nussinov, R. (2010) Zinc ions promote Alzheimer Aβ aggregation via population shift of polymorphic states. *Proc. Natl. Acad. Sci. U.S.A.* **107,** 9490–9495 CrossRef Medline
33. Hu, J.-Y., Zhang, D.-L., Liu, X.-L., Li, X.-S., Cheng, X.-Q., Chen, J., Du, H.-N., and Liang, Y. (2017) Pathological concentration of zinc dramatically accelerates abnormal aggregation of full-length human Tau and thereby significantly increases Tau toxicity in neuronal cells. *Biochim. Biophys. Acta Mol. Basis Dis.* **1863,** 414–427 CrossRef Medline
34. Huang, Y., Wu, Z., Cao, Y., Lang, M., Lu, B., and Zhou, B. (2014) Zinc binding directly regulates tau toxicity independent of tau hyperphosphorylation. *Cell Rep.* **8,** 831–842 CrossRef Medline
35. Jiji, A. C., Arshad, A., Dhanya, S. R., Shabana, P. S., Mehjubin, C. K., and Vijayan, V. (2017) Zn^{2+} interrupts R4-R3 association leading to accelerated aggregation of tau protein. *Chem. Eur. J.* **23,** 16976–16979 CrossRef Medline
36. Peskett, T. R., Rau, F., O'Driscoll, J., Patani, R., Lowe, A. R., and Saibil, H. R. (2018) A liquid to solid phase transition underlying pathological huntingtin exon1 aggregation. *Mol. Cell* **70,** 588–601.e6 CrossRef Medline
37. Patel, A., Lee, H. O., Jawerth, L., Maharana, S., Jahnel, M., Hein, M. Y., Stoynov, S., Mahamid, J., Saha, S., Franzmann, T. M., Pozniakovski, A., Poser, I., Maghelli, N., Royer, L. A., Weigert, M., *et al.* (2015) A liquid-to-solid phase transition of the ALS protein FUS accelerated by disease mutation. *Cell* **162,** 1066–1077 CrossRef Medline
38. Apicco, D. J., Ash, P. E. A., Maziuk, B., LeBlang, C., Medalla, M., Al Abdullatif, A., Ferragud, A., Botelho, E., Ballance, H. I., Dhawan, U., Boudeau, S., Cruz, A. L., Kashy, D., Wong, A., Goldberg, L. R., *et al.* (2018) Reducing the RNA binding protein TIA1 protects against tau-mediated neurodegeneration *in vivo*. *Nat. Neurosci.* **21,** 72–80 CrossRef Medline
39. Vanderweyde, T., Apicco, D. J., Youmans-Kidder, K., Ash, P. E. A., Cook, C., Lummertz da Rocha, E., Jansen-West, K., Frame, A. A., Citro, A., Leszyk, J. D., Ivanov, P., Abisambra, J. F., Steffen, M., Li, H., Petrucelli, L., and Wolozin, B. (2016) Interaction of tau with the RNA-binding protein TIA1 regulates tau pathophysiology and toxicity. *Cell Rep.* **15,** 1455–1466 CrossRef Medline
40. Rayman, J. B., Karl, K. A., and Kandel, E. R. (2018) TIA-1 self-multimerization, phase separation, and recruitment into stress granules are dynamically regulated by Zn^{2+}. *Cell Rep.* **22,** 59–71 CrossRef Medline